Environmental Pollution 396 (2026) 127858

Contents lists available at ScienceDirect

Environmental Pollution

journal homepage: www.elsevier.com/locate/envpol

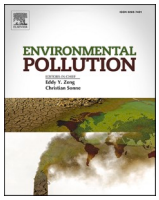

Disentangling spatial and seasonal controls on heavy metal pollution in Mediterranean rivers through fluorescence DOM☆

Alessio Polvani [a,b,c,*], Raffaello Nardin [a,b], Xinyu Liu [a,b], Francesco Di Grazia [b], Amedeo Boldrini [a,b], Riccardo Gaetano Cirrone [b,c,d], Luisa Galgani [a,b,c], Gabriella Tamasi [a,b], Steven A. Loiselle [a,b,c]

[a] Department of Biotechnology, Chemistry and Pharmacy, University of Siena, Via Aldo Moro 2, 53100, Siena, Italy
[b] Centers for Colloid and Surface Science, Via della Lastruccia 3, Sesto Fiorentino, 50019, Florence, Italy
[c] National Biodiversity Future Center, Spoke 3, University of Siena, Via Banchi di Sotto 55, 53100, Siena, Italy
[d] Department of Earth and Marine Sciences, University of Palermo, Via Archirafi 22, 90123, Palermo, Italy

A B S T R A C T

Mediterranean river basins are subject to heavy metal pollution driven by legacy mining, diffuse anthropogenic pressures, and strong hydrological seasonality. Dissolved organic matter (DOM) plays a key role in controlling metal mobility and ecological risk, while its fluorescent fraction (fDOM) provides useful optical proxies, yet its basin-scale influence remains poorly constrained. This study investigates spatial and seasonal controls on trace metal pollution across the Ombrone River Basin (central Italy), a representative Mediterranean catchment impacted by historical mercury mining. Monthly sampling along four rivers during high and low river discharge seasons combined excitation–emission matrix fluorescence spectroscopy and PARAFAC modelling with inductively coupled plasma–mass spectrometry. By combining chemometric analyses, six fDOM components, including humic-like and protein-like fractions, were evaluated alongside fifteen trace metals. A heavy metal pollution index (HPI) revealed frequent exceedances of quality thresholds, largely driven by mercury, highlighting persistent legacy contamination. Multivariate analyses showed that humic-like fDOM strongly mediated the distribution of Fe, Cu, Ni, and Se, favouring metal persistence in the dissolved phase, whereas metalloids such as Sb exhibited negative associations with humic components, indicating transport pathways dominated by mineral phases and colloids. Protein-like fDOM was linked to more transient, seasonally driven metal signals in hydrologically responsive river reaches. Overall, integrating optical fDOM properties with chemometric approaches provides a transferable framework for disentangling geogenic and anthropogenic controls on metal pollution in Mediterranean river systems.

1. Introduction

Trace metals and metalloids are ubiquitous in freshwater systems and can pose significant ecological and human health risks due to their toxicity, persistence, and potential for bioaccumulation (Tchounwou et al., 2012; Briffa et al., 2020; Ali et al., 2019). These elements enter rivers through both natural processes, such as rock weathering, and anthropogenic activities, including agricultural runoff, wastewater discharge, and legacy mining impacts (Martin and Johnson, 2012; Liang et al., 2023). Once introduced into aquatic systems, their mobility and bioavailability are significantly influenced by interactions with dissolved organic matter (DOM) (Saar and Weber, 1982; Dong et al., 2022). Optical properties of DOM, including its fluorescent fraction, provide insight into DOM composition and reactivity but do not represent bioavailability directly.

Fluorescent dissolved organic matter (fDOM) represents a dynamic subset of the total DOM pool, composed of fluorophores derived from microbial activity, plant decay, as well as anthropogenic sources, which can increase the fraction of fDOM to total DOM in impacted rivers (Wang et al., 2021). It is typically resolved into humic-like and protein-like components using excitation–emission matrix (EEM) fluorescence spectroscopy combined with parallel factor analysis (PARAFAC) (Murphy et al., 2013; Coble, 1996; Stedmon and Markager, 2005; Gabor et al., 2015). Humic-like fractions are often associated with terrestrial inputs and aromatic structures, whereas protein-like components reflect more labile, autochthonous organic matter from microbial or algal activity (Zhu et al., 2020; Mostofa et al., 2007).

The geochemical relevance of fDOM lies in its ability to complex with trace metals via carboxylic and phenolic functional groups, thereby altering metal speciation, solubility, and transport dynamics (Nguyen

☆ "This paper has been recommended for acceptance by Prof. Dr. Klaus Kümmerer".

* Corresponding author. [a]Department of Biotechnology, Chemistry and Pharmacy, University of Siena, Via Aldo Moro 2, 53100, Siena, Italy.
E-mail address: alessio.polvani@student.unisi.it (A. Polvani).

https://doi.org/10.1016/j.envpol.2026.127858
Received 23 December 2025; Received in revised form 2 February 2026; Accepted 19 February 2026
Available online 20 February 2026

et al., 2024; Baken et al., 2011; Poulin et al., 2014). Metals such as copper, lead, and mercury can form strong organo-metallic complexes with DOM, which typically reduces their bioavailable fractions and toxicity (Kikuchi et al., 2017; Li et al., 2023; Yamashita and Jaffé, 2008; Zhang et al., 2021).

Understanding fDOM–metal interactions is therefore critical for improving ecological risk assessments and for interpreting pollutant dynamics under different hydrological conditions (Li et al., 2024). These interactions modulate the retention, transformation, and downstream export of trace metals—particularly during episodic events like storms or seasonal runoff, which alter DOM composition and concentration (Bhattacharya and Osburn, 2021). In catchments affected by diffuse pollution or legacy mining, DOM-driven complexation can either enhance or inhibit the transport of metal contaminants (Liang et al., 2023).

The development of real-time fDOM monitoring tools has expanded opportunities for tracking contamination events and evaluating water quality trends. Spectroscopic characterization of fDOM is now recognized as a rapid, cost-effective, and informative technique for identifying pollution sources and metal–organic interactions under dynamic flow regimes (Bieroza and Heathwaite, 2015; Chen et al., 2023; Tedetti et al., 2013).

This work contributes to the EU Mission *"Restore our Ocean and Waters by 2030"*, which promotes integrated monitoring and pollution mitigation across the land–sea continuum (European Commission, 2023). River basins in the Mediterranean-such as the Ombrone-play a key role in controlling the transfer of contaminants to coastal waters, highlighting the need for robust indicators of chemical pressure and transport processes. By addressing trace metal–fDOM interactions under variable hydrological conditions, this study supports new insights into the sustainable management of Mediterranean river basins with complex history of mining and land use. Specifically, the study adopts an integrated basin-scale framework that combines optical DOM characterization with complementary statistical analyses to disentangle spatial and seasonal drivers of metal concentrations.

In this context, the objectives of this study are:

1. To explore the links between heavy metal concentrations and fDOM dynamics in relation to local sources and sinks, and considering seasonal hydrological variability;
2. To evaluate the ecological risk associated with heavy metals in surface waters in combination with fDOM composition; and
3. To identify predictor variables, including river basin characteristics and seasonal hydrological indicators, as robust proxies for heavy metal pollution and mobility in river systems.

2. Materials and methods

2.1. Study area and sampling collection

The Ombrone River Basin (ORB), located in central Italy, represents a typical Mediterranean catchment, encompassing diverse geological, hydrological, and land-use characteristics over its 3500 km^2 area (Frangipane and Paris, 1994). The region experiences a distinctly seasonal hydrological regime, with high flows in autumn and spring and markedly reduced river discharges in summer (Thornes et al., 2009; Benito et al., 2015). The Ombrone River itself stretches for 161 km before reaching the Tyrrhenian Sea and is known for transporting high suspended sediment loads relative to other regional rivers. Land cover in the basin is dominated by woodland and agricultural zones (Sanna et al., 2025), interspersed with small population centers totalling approximately 280,000 inhabitants (Italian National Institute of Statistics ISTAT, 2021). Historically, the ORB has undergone extensive mining activity, dating back to Etruscan times and continuing into the 20th century (Dini et al., 2024). The basin is dominated by Mt. Amiata, a Quaternary volcanic complex, which hosts one of the world's largest cinnabar deposits. Although mining ceased in the late 20th century, the weathering of mineralized substrates and remobilization of historical mine wastes continue to contribute Hg and associated trace elements to tributaries draining toward the Orcia River, influencing basin-scale contamination patterns (Fornasaro et al., 2022; Chiarantini et al., 2016).

Sampling was conducted on four rivers in the ORB over the periods of high and low river discharge seasons in 2024 and 2025. High and low discharge were estimated based on monthly precipitation totals obtained from the regional environmental agency (Servizio Idrologico Regionale della Toscana, 2024). In each river, Ombrone, Farma, Merse, and Orcia (hereafter referred to as Om, F, M, and Or, respectively, when discussing sampling sites), sampling was performed monthly over four consecutive months. Sites were selected along each river, to represent longitudinal gradients of potential natural and anthropogenic influences, from headwaters to downstream sections. In total, triplicate samples from 26 sites were obtained, along with local observational characteristics (riparian vegetation, local land use, presence of algal blooms, water colour) (Bishop et al., 2025) (Fig. 1). Water was collected just below the surface to avoid disturbance of bottom sediments and surface organic matter films.

2.2. Laboratory analysis

2.2.1. fDOM analysis

Three-dimensional excitation–emission matrices (EEMs) were acquired and analysed using Parallel Factor Analysis (PARAFAC) to characterise fDOM. For this purpose, 15 mL of water were filtered *in situ* through 0.22 μm PTFE membrane filters (VWR), stored refrigerated at 4 °C and in the dark, and analysed within 24 h (n = 267). EEMs were recorded using a Cary Eclipse spectrofluorometer (Agilent) equipped with 1 cm quartz cuvettes. Excitation wavelengths ranged from 200 to 450 nm at 10 nm intervals, while emission wavelengths spanned 250–600 nm with a 2 nm data interval. Instrument settings included 5 nm excitation and emission slit widths, a scan rate of 1200 nm/min, and a photomultiplier tube voltage of 600 V. Raw fluorescence data were processed in MATLAB (R2022b) using the drEEM toolbox. Processing steps included blank subtraction using freshly produced ultrapure water (Milli-Q, Millipore, Darmstadt, Germany), removal and interpolation of Rayleigh and Raman scattering regions, and normalisation of EEMs to total fluorescence intensity to minimize concentration-related effects. PARAFAC modelling was applied to the corrected EEM dataset to decompose fluorescence signals into independent components, with component intensities expressed in arbitrary units. Outliers were identified using Mahalanobis distance and evaluated for influence prior to final model selection.

2.2.2. Trace metal analysis

For trace metal analysis, samples were taken at the same time as fDOM samples and stored under the same conditions but without in-situ filtration. The following day, samples were centrifuged (4 min at 4000 rpm) to minimize suspended particulates, acidified with ~1% ultra-pure HNO_3 (re-distilled, 99.9999% metal trace basis acquired by Merck KGaA), and then filtered with 0.22 μm PTFE membrane metal-free filters (VWR). Fifteen metals were selected due to their relevance as common environmental contaminants (Al, Cr, Mn, Fe, Ni, Cu, Zn, As, Se, Cd, Sb, Ba, Hg, Tl, Pb). Metal concentrations were determined using an Agilent 8900 ICP-MS triple quadrupole equipped with a quartz shielded torch with a 2.5 mm injector and Ni-Cu interfaces cones. Internal standard (Y, Ge, Rh) solution obtained by dilution of stock solutions (1000 mg/L, acquired by Merck KGaA) were added to the samples at a final concentration of 50 μg/L to monitor plasma fluctuation. Samples were introduced using an Agilent SPS 4 Autosampler connected to a quartz nebulizer (MicroMist – Agilent) and inserted into a quartz Scott spray chamber cooled to 2 °C by a Peltier module.

6-points calibration curves were obtained by dilution of a stock solution (10 mg/L, acquired by Merck KGaA) in the range 10 ng/L-100 μg/

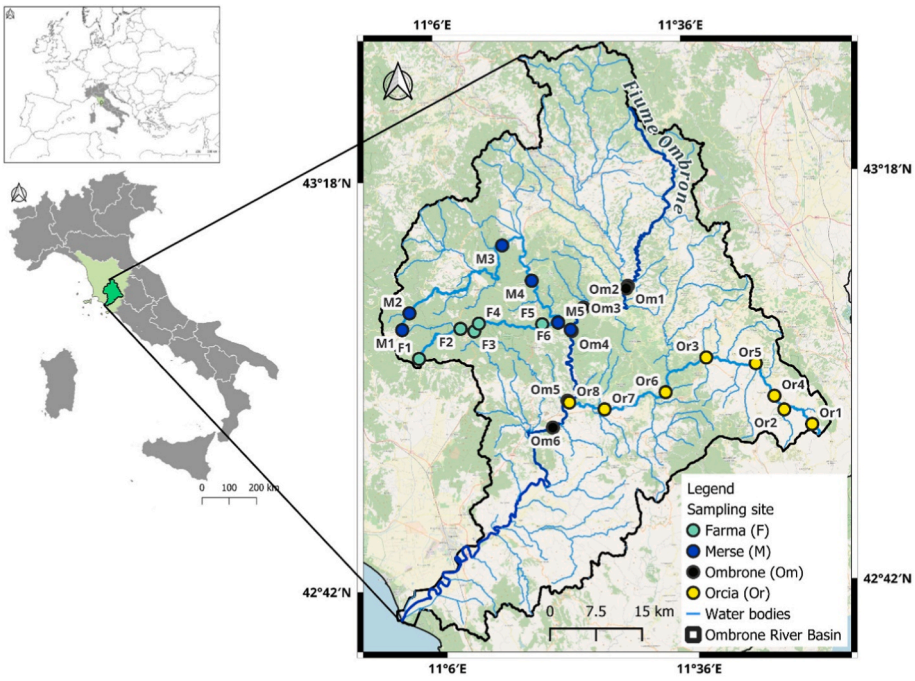

Fig. 1. Study area and sampling sites within the ORB.

L defined based on the concentrations typically observed in the samples. All measurements were performed in triplicate. Limits of Detection (LoD) for Al, Cr, Mn, Fe, Ni, Cu, Zn, As, Se, Cd, Sb, Ba, Hg, Tl, Pb were respectively 0.2, 0.016, 0.051, 0.3, 0.029, 0.014, 0.001, 0.005, 0.004, 0.02, 0.063, 0.015, 0.022 and 0.017 μg/*L*. LoD were calculated as 3σ/S where σ is the standard error and S the slope of the calibration curve. Typical operating parameters and instruments specifics are reported in Supplementary Materials (Table S1). Elements were analysed by introducing either He or O2 in the octapole to remove isobaric interferences by either collision (He Mode) or by using the M+ + O2 → MO+ + O reaction (O2 Mode). Integration time and reaction parameters for each element analysed can be found in Supplementary Materials (Table S2).

2.2.3. Water quality indexes

A heavy metal pollution index (HPI) was calculated by considering the concentrations of all fifteen metals determined for each site (Al, Cr, Mn, Fe, Ni, Cu, Zn, As, Se, Cd, Sb, Ba, Hg, Tl, Pb), weighted by relative toxicity (Badeenezhad et al., 2023). For each metal *i*, a regulatory limit S_i for surface waters (μg/*L*) were obtained from the Annual Average Environmental Quality Standards (AA-EQS) set by European Water Framework Directive (WFD) and from ARPAT (Regional Agency for Environmental Protection of Tuscany) tap water regulations; where limits were unavailable, World Health Organization (WHO) drinking-water guidelines were used (Table S3) (European Commission, 2008; ARPAT, 2023; World Health Organization, 2022). Mean concentrations per sample (considering triplicate sampling and triplicate determination) were used. The relative weight of each metal was assigned following the weighted arithmetic index method. Unit weights W_i were calculated as:

$$W_i = \frac{k}{S_i}$$

where

$$k = \left[\sum_{i=1}^{n}\left(\frac{1}{S_i}\right)\right]^{-1}$$

ensuring $\sum W_i = 1$. Smaller regulatory limits therefore correspond to higher weights (Table S3).

The quality rating Q_i for each metal was expressed as the percentage of its limit:

$$Q_i = \left(\frac{C_i}{S_i}\right) \times 100$$

where C_i is the mean measured concentration at the site. Because toxic metals ideally occur at zero concentration, the ideal value was set to 0. The sub-index (SI) for each metal was then obtained as:

$$SI_i = W_i \times Q_i$$

and the HPI at each sample was computed as the sum of all sub-indices:

$$HPI = \sum_{i=1}^{n} SI_i$$

The HPI value below 100 was set to indicate non-contaminated water, while a value above 100 suggests a contamination by heavy metals (Badeenezhad et al., 2023). HPI formulations are not universally standardised, as the index reflects the specific suite of metals measured within the local context.

Another key indicator calculated to assess the river water quality is the ratio of protein-like (tryptophan and tyrosine like fDOM) to humic-like fDOM (humic and fulvic like fDOM) (T/C ratio). This index has been used to identify fDOM sources and pollution events in multiuse river basins (Liu et al., 2025). The relative intensities of the protein-like components (C4 and C6), representing tyrosine- and tryptophan-like fluorescence, were summed and divided by the combined intensities of the humic-like and fulvic-like components (C1, C2, and C3), following the equation:

$$\mathrm{T}\Big/\mathrm{C\ ratio} = \frac{C4 + C6}{C1 + C2 + C3}$$

Higher values indicate a greater proportion of microbially derived, and labile material, often associated with recent biological activity or anthropogenic inputs (e.g., wastewater or agricultural runoff). Conversely, lower ratios reflect the dominance of more humified, refractory organic matter typically derived from terrestrial sources (Liu

et al., 2025). Tracking variations in the T/C ratio across sampling sites and seasons was used to evaluate changes in water quality, microbial productivity, and the influence of allochthonous versus autochthonous organic inputs within the river system.

2.2.4. Statistical analysis of fDOM and metal dynamics

The analyses of the relationships between metals and between metals and fDOM was performed using the full dataset consisting of trace metals, fDOM components (C1–C6) and the water quality indexes. For the analyses, to ensure that all variables had a similar variance, all values of each variable were normalized using Z-scores.

Correlation analysis (Spearman) carried out in R software (R 4.4.0) was performed to quantify linear associations among metals, fDOM components, and the T/C ratio, allowing identification of covariance and to construct a correlation network.

To explore the relationships between individual fDOM components under metal-enriched conditions, binary logistic regression (LR) models were applied using each PARAFAC component and the T/C ratio. fDOM components were binarized considering the distribution of fDOM conditions measured in the ORB. For each component, an LR model was fitted independently, and performance was evaluated using overall accuracy and the Area Under the Receiver Operating Characteristic Curve (AUC).

Based on the LR results of significant fDOM-metal relationships, overall trend of metal concentrations with increasing fDOM values was explored using fDOM quartiles and Kruskal–Wallis, to evaluate whether metal concentrations changed systematically across increasing fDOM components, using pairwise Mann–Whitney U tests as a follow up test.

Discriminant analysis (DA) was applied to explore multivariate chemical differences among rivers, conducting a MANOVA to obtain the within-group (E) and between-group (H) sum-of-squares and cross-products matrices, from which discriminant functions were derived using the eigen decomposition of $E^{-1}H$. Because nearly all metals exhibited strong skewness (skewness >2), a rank transformation was applied prior to DA to reduce the influence of extreme values and relax distributional assumptions while preserving relative differences among samples. Discriminant scores were calculated for each sample and averaged to obtain river centroids. Variable loadings for each metal and fDOM component and correlations with discriminant scores were used to identify the chemical variables driving river separation.

To identify longitudinal trends in fDOM and metal concentrations along each study river, the non-parametric Mann–Kendall test was applied to assess the significance of monotonic changes from headwaters to the downstream sampling locations.

3. Results

3.1. fDOM distribution

PARAFAC modelling of excitation–emission matrices (EEMs) was used to identify independent fluorescent components of DOM. The optimal number of PARAFAC components was determined by sequentially evaluating models with five to seven components, based on a combination of residual analysis, split-half validation, component stability, and chemical interpretability. Five component models resulted in the merging of chemically meaningful fluorophores with artefactual features, whereas seven component models produced duplicated ("split") components with highly similar excitation–emission characteristics, indicative of overfitting. The six component solution represented the most parsimonious model that maximized explanatory power while retaining physically meaningful and stable fluorescent components (Fig. 2).

Component 1 exhibited maxima at Ex/Em = 250/408 nm, typically associated to humic-like substances of terrestrial origin with relatively less humified material (Linlin et al., 2011). Component 2 (Ex/Em = 250/476 nm) corresponded to a more red-shifted, fulvic-like emission

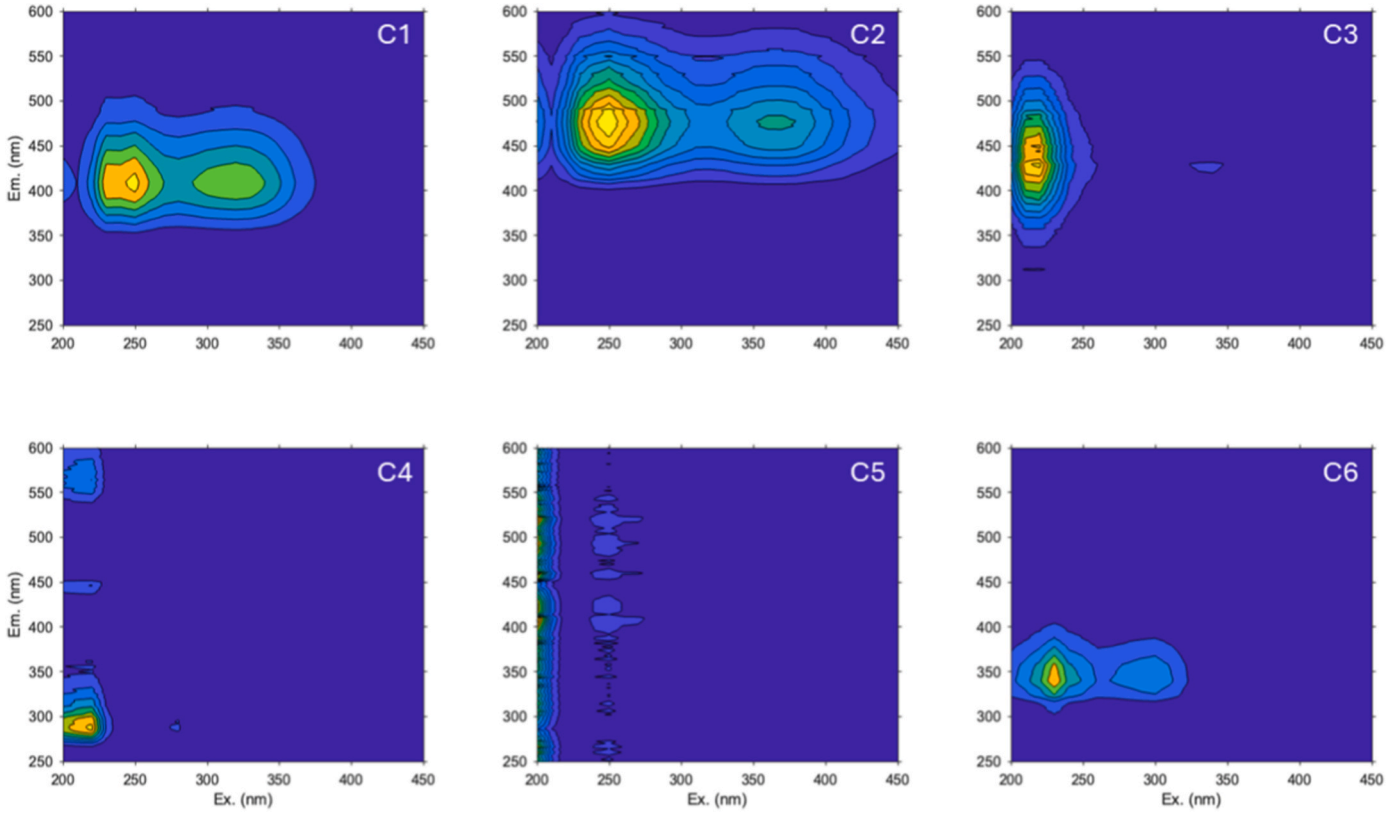

Fig. 2. Six fDOM components obtained from the PARAFAC model, consisting of three humic/fulvic-like components (C1, C2, C3; top row), two protein-like components (C4 and C6), and one unidentified noise component (C5; bottom row).

(peak C/C+), indicative of highly humified DOM. Component 3 (Ex/Em = 220/430 nm), also falls within the humic-like (A/C) region, reflecting a short-wavelength excitation band typical of aromatic terrestrial fluorophores (Derrien et al., 2020; Lin et al., 2021). Component 4 (Ex/Em = 220/288 nm) and Component 6 (Ex/Em = 230/344 nm) were identified as protein-like components, corresponding to tyrosine-like and tryptophan-like DOM, respectively (Chen et al., 2022; Yan et al., 2020). Both are generally associated with autochthonous, microbially derived, and labile organic matter (Coble, 1996; Guo et al., 2010). The fifth component, characterized by a strong vertical feature centred around Ex ≈ 200 nm, was considered noise and excluded.

Mean PARAFAC component scores revealed seasonally variable fDOM characteristics of the four rivers (Fig. 3). In the Orcia River, none of the fluorescent components exhibited statistically significant seasonal variation using pairwise Mann–Whitney U tests ($p > 0.01$), indicating relatively stable fDOM composition across discharge conditions. In contrast, the Merse River showed pronounced seasonal shifts, with significantly higher intensities of the protein-like components and lower humic-like intensities during the low-discharge season. The Farma River followed a similar trend. The Ombrone River displayed a similar pattern for protein-like fluorescence but no significant differences for humic-like components.

The Orcia River had the highest mean total fluorescent intensity but the lowest T/C ratio (0.30), indicating dominance of humic-like components (C1–C3) and the lowest protein-like intensities (C4 and C6) (Fig. 3; Table S4)

By contrast, the Merse River showed the highest mean intensities of protein-like components, yielding the highest T/C ratio (0.86), with values exceeding 1 at sites M2 and M3.

The Ombrone and Farma rivers displayed intermediate humic and protein signatures, with mean T/C ratios of 0.44 and 0.63, respectively. Notably, the Ombrone River exhibited a strong downstream increase in the T/C ratio (Fig. S1): the upper sites (Om1–Om3) averaged 0.21, while the lower sites (Om4–Om6) averaged 0.64. The lower sites are downstream of the confluence with the Merse River, which confirmed the influence of this tributary.

The Farma showed a reduction in the T/C ratio, initially above 0.9 in the upstream sites (F1–F2) and progressively decreasing downstream, consistent with slow, sometimes stagnant headwaters that enhance algal growth and protein production (Fig. S1). The Orcia river demonstrated a significant positive trend (Mann-Kendall $p = 0.018$) with increasing distance from the headwater site.

Sampling was performed over two periods, during months of high river discharge (spring and autumn) and low river discharge (summer). High and low discharge conditions were estimated based on mean monthly precipitation totals. The average monthly precipitation for the high discharge period was 58.7 mm ± 16.5 mm, while that for the low discharge was 27.9 mm ± 6.4 mm, consistent with the Mediterranean seasonal hydrological regime. T/C ratios were higher in low river discharge periods (0.78) than in high discharge period (0.38), reflecting a higher proportion of protein-like fDOM in drier, warmer months (Table S5), consistent with trends reported in similar studies (Ma and Li, 2020; Mohinuzzaman et al., 2025; Wang et al., 2022).

3.2. Metal content in ORB rivers

The average metal concentrations measured across the sampling sites show a clear geographic distribution of concentrations (Table S6). For key metals—Ni, Cd, Cr, and Pb—the mean concentrations at all sampling sites were below the annual average threshold set by environmental quality standards (AA-EQS) according to the WFD for surface waters (20, 0.08, 50 and 7.2 μg/*L*, respectively).

A markedly different picture emerges for Hg. On average, half of the sampling sites (13 out of 26) exhibited Hg concentrations exceeding the AA-EQS of 0.03 μg/*L*. The Farma and Orcia rivers consistently surpassed this limit, whereas the Merse and Ombrone rivers did not. The high river discharge periods in both the Farma and Orcia rivers showed particularly high values, with mean concentrations almost an order of magnitude above the EQS (Table S5). All sampling points along the Farma River exceeded the limit, while no exceedances were recorded along the Merse River.

For the other metals, none exceeded typical limits for either surface or tap water. Exceptions were Fe and Mn: Fe reached an average of 257 μg/*L* (limit: 200 μg/*L*) in the Merse, and Mn reached of 430 μg/*L* in the Orcia (limit: 50 μg/L for tap water; no environmental threshold available). M2 also exhibited periods of elevated Cu and Al, although their average concentrations did not exceed their respective limits or guidelines.

Highest HPI values were observed at sites F1 and Or1, with values of 677.78 and 680.72, respectively. In total, nine sites exceeded the commonly accepted HPI threshold for good water quality (>100), including all six sites along the Farma River (F1 to F6) and the three upstream sites of the Orcia River (Fig. 4). Among these, the Farma River exhibited the highest average HPI values across its course, although a decreasing trend was noted from upstream (F1) to downstream (F6).

In the Orcia River, a pronounced difference was observed between Or1 and Or2, largely driven by a mercury concentration of 1.11 μg/L recorded at Or1 during the May sampling campaign. In contrast, in the

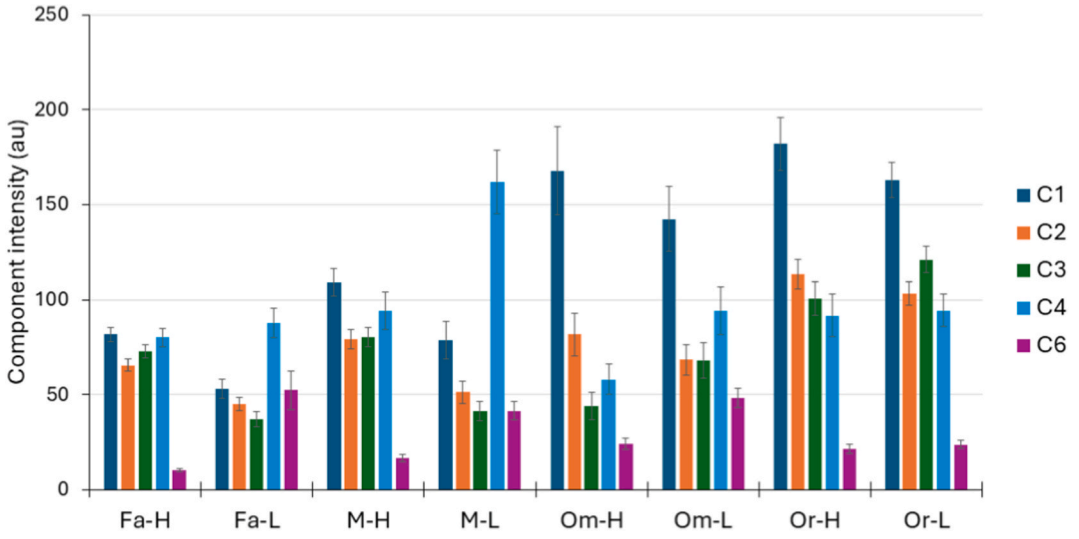

Fig. 3. fDOM components average intensity (au) per river and high (H) or low (L) river discharge seasons.

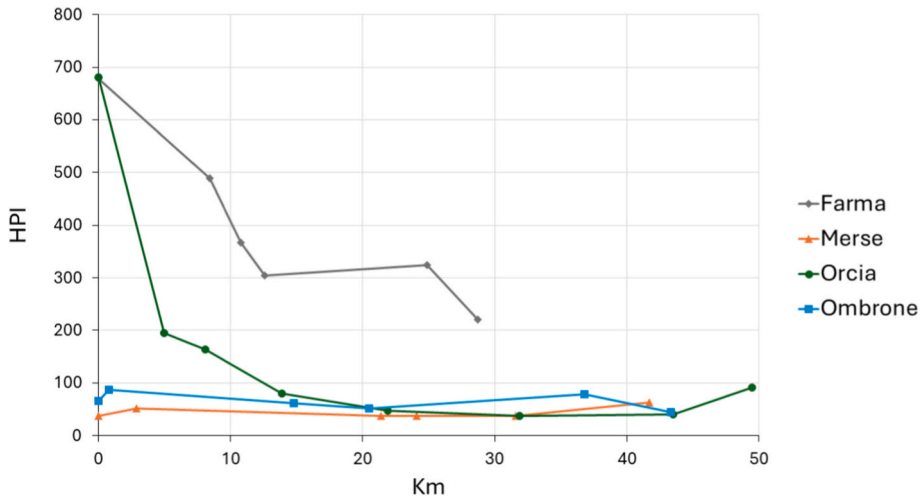

Fig. 4. Longitudinal change in HPI for each river.

Farma River, exceedances of the HPI threshold were consistently recorded across multiple sampling events, suggesting a more persistent contamination pattern.

The Merse River displayed the lowest HPI values among the four rivers. A localized increase at M2 is attributable to inputs from the Ribudelli Creek, which drains the former mining site at Campiano and introduces metals into the main channel. A subsequent decline in HPI at M3 reflects dilution effects from the mainstem flow. A modest rise at M6 is likely influenced by the confluence with the Farma River upstream, which, as noted, consistently displays elevated mercury levels.

The Ombrone River showed intermediate HPI values overall. However, most of its sampling sites remained below the pollution threshold on average. The Kruskal–Wallis test revealed statistically significant differences in HPI among sites in the Merse and Orcia rivers, whereas no significant differences were detected in the Farma and Ombrone rivers.

These HPI patterns reinforce the dominant influence of mercury in determining overall water quality status within the basin. Notably, mercury accounts for approximately 70% of the HPI calculation (Table S3), amplifying the impact of elevated concentrations at specific sites and highlighting legacy contamination as a key factor affecting the ecological health of these systems.

3.3. Metals and fDOM dynamics

The correlation network (Fig. 5) revealed a cluster of lithogenic and redox-sensitive metals (Fe, Al, Mn, Ni, Cu, Ba), connected by strong positive correlations, with Fe at the centre. This pattern reflects (i) the highly erodible geology of the basin, (ii) Fe–Al–Mn signatures associated with pyrite mineralization in the Merse River, and (iii) the neutral-to-alkaline pH conditions typical of these rivers (ARPAT, 2022). Ni mobility increases in the presence of Mn and Fe oxides, leading to higher dissolved Ni concentrations where such oxides form or mobilize (Rinklebe and Shaheen, 2014).

Regarding the relationship between fDOM and metals, Fe and Cu were positively correlated with components C1 (Spearman's $\rho = 0.471$) and C2, consistent with the tendency of Cu(II) to complex with terrestrial humic components (Yang et al., 2026). Metal associations in the Merse–Farma system are likely to be influenced by historic mining and sulphide mineralization which have shown elevated As, Cu, Pb, Zn and Fe concentrations in biological species (Monaci et al., 2021). Our analysis confirmed high concentrations of Fe, Cu, Zn and As in these rivers, as well as correlations between Fe with Cu and As, as well as between Pb and Zn (Table S6).

On the other hand, metalloids as Sb showed a strong negative correlation with all humic-like components, suggesting that Sb-enriched

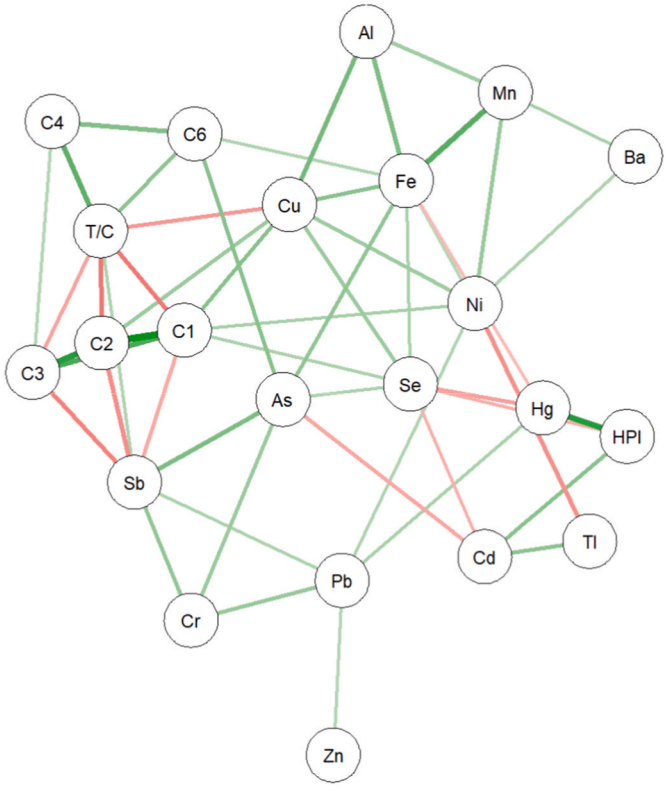

Fig. 5. Spearman's correlation network. Line colour denotes the sign of the correlation (green = positive, red = negative), while thickness reflects correlation magnitude ($|\rho|$). Only medium or stronger correlations ($|\rho| > 0.3$, Cohen's criteria) significant at $p < 0.01$ are shown. (For interpretation of the references to colour in this figure legend, the reader is referred to the Web version of this article.)

pulses arising from (i) acid mine-drainage inputs into the Merse River, where Fe-driven oxidative weathering mobilizes metalloids from sulfide deposits, and (ii) geogenic–volcanic sources in the Orcia basin (Pagnanelli et al., 2004; Nannoni et al., 2025). Metalloids may be transported via Fe- and Al-rich colloids rather than humic-bound pathways, especially under alkaline pH conditions (Yang et al., 2021).

Protein-like components behaved differently; C4 showed no significant correlations with metals, while C6 exhibited a strong positive correlation with As (Spearman's $\rho = 0.468$), similar to Zhu et al. (2024)

as well. Wang et al. (2015) reported that protein-like components dominated the interactions between the DOM and the four metalloid ions with the following affinity order was Sb(III) > As(III) > As(V) > Sb (V).

Liang et al. (2023) similarly highlighted the strong affinity of As, Se, and Cd with protein-like fDOM with higher aromaticity in Yangtze River sediments.

The contrasting behaviour of As and Sb relative to humic-like fDOM observed in this study is consistent with their anionic speciation and reduced affinity for classical humic binding sites, as well as competition-driven partitioning under metal-rich conditions. Conversely, the strong association of Cu with humic-like components reflects its high affinity for organic ligands, widely documented in mining-impacted river systems. As reported by Liu et al. (2024), the complexation between Cu(II) and DOM may facilitate the microbial breakdown of fDOM, especially the protein-like components, resulting in T/C ratio modification.

The associations between metal concentrations and specific fDOM components were further explored using multivariable logistic regression, with z-score-normalized metal concentrations as predictors of binary high/low fDOM fractions. Model coefficients were used to evaluate conditional associations while controlling co-variation among metals. Metals showing significant positive coefficients interpreted as being associated with the probability of elevated levels of each fDOM component.

Model performance was evaluated using the area under the receiver operating characteristic curve (AUC), which quantifies the ability of each model to discriminate between high and low fDOM conditions. AUC values can range from 0.5 (random classification) to 1.0 (perfect separation), with >0.8 typically denoting strong predictive utility in the classifiers. Models for all fDOM components except C4 showed strong discriminatory performance, with AUC values exceeding 0.80. Among these, the short-excitation humic component C3 exhibited the highest classification performance (AUC = 0.89), followed by C1 and C2 (AUC = 0.87 and 0.83, respectively). In contrast, the tyrosine-like C4 component showed weak discriminatory power (AUC = 0.69), consistent with its short residence time and limited involvement in metal complexation (Cory and Kaplan, 2012). C6 also demonstrated strong discriminatory performance (AUC = 0.84).

Metal-specific coefficients from the multivariable logistic regression revealed distinct associations between individual fDOM components and specific metals. Cu showed significant positive associations with elevated humic-like fDOM components C2 and C3, and a negative association with the T/C ratio, indicating a preferential association with humic relative to protein-like DOM. Ni, together with Ba, exhibited significant positive associations with C1, further supporting the affinity of these metals for humic-like fDOM. In contrast, Al was positively associated with the T/C ratio, suggesting that higher Al concentrations are more likely under conditions characterized by a greater relative contribution of protein-like fDOM. Across the full dataset, As and Fe emerged as significant positive predictors of elevated tryptophan-like fluorescence (C6), indicating a preferential association with protein-like fDOM components under specific conditions. Multicollinearity was low (Variance Inflation Factor <2 for all metals except Al and Fe, 5.5 and 5.2 respectively) confirming stable coefficient estimates and model reliability.

Following the logistic regression, changes in metal concentrations across increasing fDOM quartiles were evaluated to identify concentration ranges associated with the observed associations. For all cases shown, metal concentrations differed significantly among fDOM quartiles (Kruskal–Wallis, $p < 0.05$).

Significant positive relationships between metal concentrations and fDOM were observed for Cu, Fe, As, and Ni when samples were grouped by fDOM quartiles across all rivers and seasons. Cu concentrations increased with increasing humic-like fDOM components C2 and C3, in agreement with the positive coefficients identified in the logistic regression models (Fig. 6a). A similar response was observed for Fe and As in relation to the tryptophan-like component C6 (Fig. 6b), reflecting pooled, dataset-wide associations that may arise from episodic or river-specific processes. While no statistically significant differences were detected between the first and second C6 quartiles for either metal, increases occurred between the second and third quartiles, as confirmed by Mann–Whitney tests ($p < 0.05$), with Fe concentrations rising from 8.23 to 19.39 $\mu g/L$ and As from 0.42 to 0.96 $\mu g/L$. Ni also showed increasing concentrations across quartiles of component C1, with median values rising from 0.40 to 0.85 $\mu g/L$, consistent with its positive association with humic-like fDOM identified in both correlation and logistic regression analyses.

In contrast, several metals displayed negative associations with increasing fDOM. Sb exhibited consistently negative relationships with humic-like components, in agreement with negative correlations and

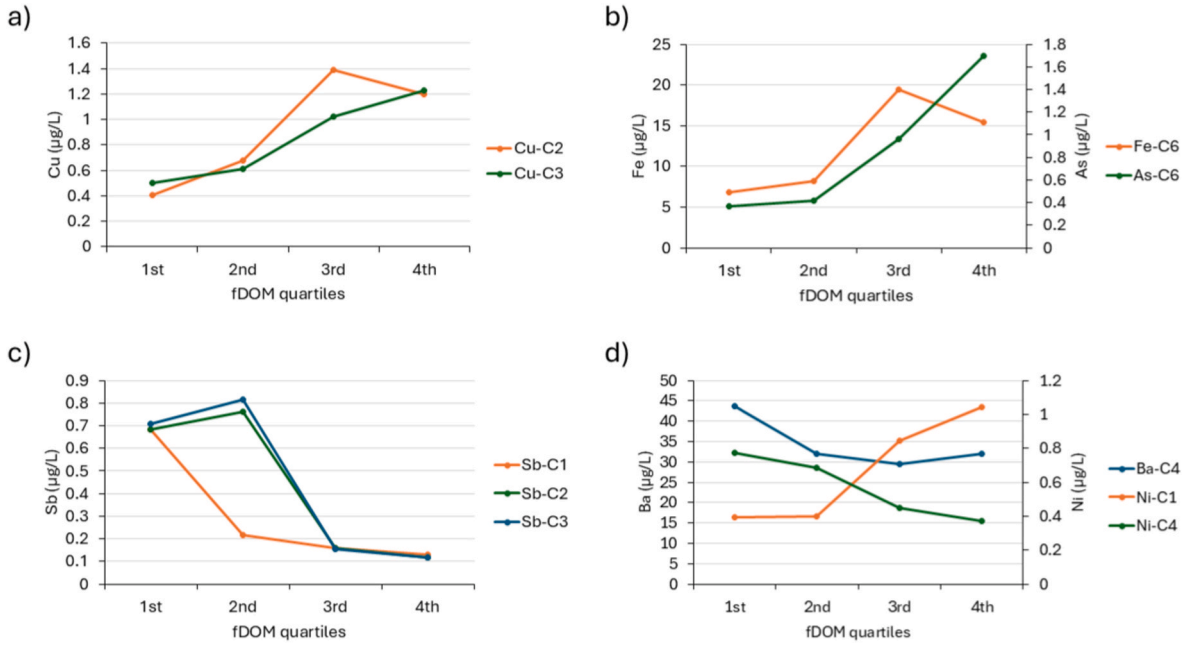

Fig. 6. Median metal concentrations across fDOM quartiles showing significant differences (Kruskal-Wallis test, $p < 0.05$).

logistic regression coefficients (Fig. 6c). Across components C2 and C3, Sb concentrations remained relatively high at low fDOM levels but declined sharply at higher quartiles, with median values decreasing from >0.6 μg/*L* in the lower quartiles to approximately 0.2 μg/ *L* in the upper quartiles. For component C1, a similar decline occurred earlier, with Sb concentrations decreasing between the first and second quartiles. These stepwise decreases were supported by significant pairwise differences between quartiles (Mann–Whitney tests, $p < 0.05$).

Ni also exhibited a negative response to increasing fDOM for the tyrosine-like component C4, with median concentrations decreasing from 0.68 to 0.45 μg/*L*, consistent with the negative coefficient observed in the logistic regression model (Fig. 6d). A comparable pattern was observed for Ba and component C4, where a strong and statistically significant decrease occurred between the first and second quartiles (median concentrations declining from 43.66 to 31.90 μg/ *L*), followed by a plateau at higher fDOM levels, with no further significant differences detected between subsequent quartile

3.4. Basin scale and seasonal dynamics

The four basins were shown to differ significantly when considering individual and combined metal concentrations and fDOM content (Table S4 and Table S6, ANOVA and MANOVA, p-value <0.001). To explore how metal concentrations and fDOM could be used to separate river basins across seasons of high and low precipitation, an exploratory discriminant analysis was used in a canonical framework. Highly correlated humic fDOM components (C1, C2, C3) were combined into a single humic-like component, and C4 and C6 components into a single protein like component. Samples were grouped by river and hydrological season (high and low river discharge), and DA was used to examine multivariate separation among groups. The resulting model showed a total accuracy of 82%, with individual rivers ranging from the Merse with an average accuracy of 74% to the Ombrone at 94%. Given that there was a strong heterogeneity of covariance matrices among seasonal river conditions (Box's M test, $p < 0.0001$), discriminant function coefficients were not interpreted. Instead, river centroids were used to describe multivariate patterns of separation between rivers and seasons (Kannel et al., 2007).

The first two discriminant functions explained 80% of the total between-river variance (DF1 = 55%, DF2 = 25%) (Fig. 7). DF1 primarily reflected spatial separation among river basins, with Orcia clearly separated from the other rivers, while seasonal differences within each river were small relative to between-river differences. In contrast, DF2 captured river-specific seasonal variability, which was most pronounced in the Ombrone, whereas Farma, Merse, and Orcia showed comparatively stable positions across seasons.

The relationships between the two fDOM types and metals in the first two discriminant functions reflect basin-scale multivariate patterns that maximize separation among rivers and seasons. At this scale, humic-like fDOM was strongly associated with Fe, Cu, Se, and Ni, indicating that organically complexed or soil-derived metals contribute consistently to the chemical differentiation among river basins. In contrast, protein-like fDOM showed positive associations with Mn and Al, suggesting a weaker linkage with trace metal transport and a greater influence of biologically labile or shallow-soil processes on river-specific signatures (Fig. 8).

Overall, the DA showed contrasting metal–fDOM regimes between rivers. The Orcia was characterized by strong associations between humic-like fDOM and Fe, Cu, Se, and Ni, suggesting metal complexation and transport in organic-rich waters that remain relatively stable across seasons. In contrast, the Merse and its tributary Farma display metal patterns that are weakly coupled to humic fDOM and instead dominated by elements such as Sb, Ba, and, in the case of Merse, Fe and Cu, suggesting transport pathways that are controlled primarily by mineral phases and sediments. The Ombrone shows a different behavior, with pronounced seasonal shifts in discriminant space linked to summertime increases in protein-like fDOM and concurrent variations in Zn, Ba, and Sb. Persistent differences in DOM–metal characteristics between rivers dominated, with seasonality acting as a secondary, basin-specific modifier.

4. Conclusion

By integrating multiple approaches: correlation networks, rank based inference testing, multivariable logistic regression, and discriminant analysis, this study provided an integrated picture of the spatial and seasonal variability of metal concentrations and their potential interaction with fDOM. All approaches consistently identified humic-like fDOM as a potential mediator of metal mobility, particularly for Fe, Cu, Ni, and Se, whereas metalloids such as Sb and, to a lesser extent, As exhibited contrasting behavior indicative of transport pathways dominated by mineral phases and colloids rather than classical humic complexation. These commonalities across independent analytical frameworks suggest robustness of the observed metal–fDOM coupling regimes and reduce uncertainty associated with any single method.

DA further demonstrated that river-specific characteristics, legacy mercury mining in Orcia and Farma, pyrite and sulfide mineralization in Merse and Farma, greater hydrological buffering in Orcia and Merse, and higher responsiveness in Ombrone, exert stronger control on water chemistry than seasonality, with persistent basin differences dominating contrasts between high and low river discharge periods in three of the four rivers. Seasonal effects were nevertheless evident in hydrologically responsive systems, in particular the main Ombrone River, where shifts toward protein-like fDOM occurred in the high river discharge season. Together, these results indicate that changes in the balance between humic-like and protein-like fDOM influence metal transport pathways, with humic-dominated conditions favoring metal complexation and persistence in the dissolved phase, and protein-rich conditions reflecting more transient, biologically or runoff-driven inputs.

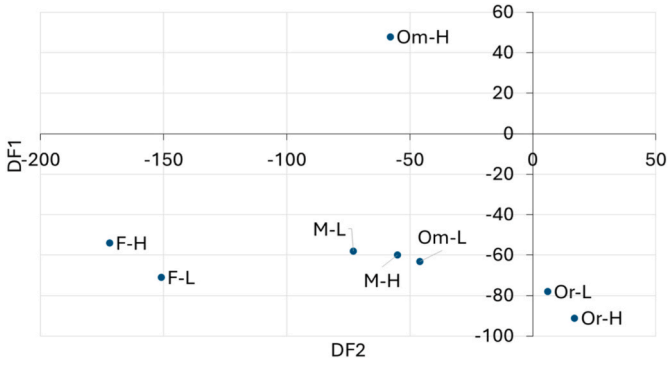

Fig. 7. DA centroid plot for different rivers and season (H: high precipitation and river discharge, L: low precipitation and river discharge).

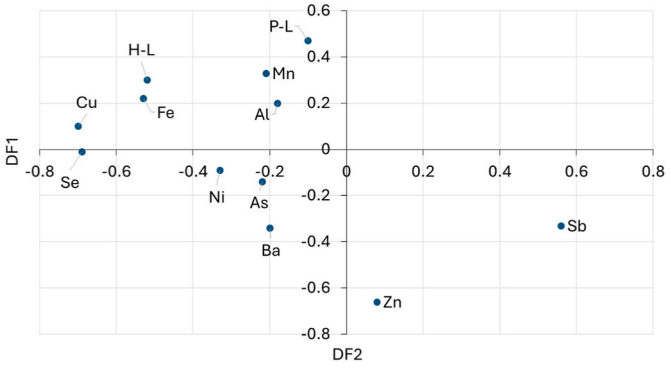

Fig. 8. DA plot of metal and fDOM (H-L as humic-like fDOM, P-L as protein-like fDOM).

The consistency of results highlights the broader applicability of this framework for investigating metal pollution dynamics in river systems subject to mixed pressures, including legacy and active mining, agriculture, and population centers. By integrating fDOM optical properties with multivariate metal patterns, this approach allows disentangling geogenic from anthropogenic signals and identifying river reaches where seasonal processes amplify or attenuate metal mobility. Such integrative analyses are particularly relevant for Mediterranean-type catchments, where increasing intense and episodic hydrological events combine with long histories of land use to shape water quality.

Finally, the elevated HPI values observed in several river sections, largely driven by mercury, underscore the persistence of legacy contamination and its potential downstream implications. Given that these rivers ultimately discharge into the Mediterranean Sea, continued metal transport under humic-rich conditions may contribute to coastal metal loading and ecological risk, reinforcing the need for basin-scale monitoring strategies that explicitly consider fDOM–metal interactions. The methodological framework presented here offers a transferable tool for assessing metal pollution risks and their controlling processes in other riverine systems draining sensitive coastal environments.

CRediT authorship contribution statement

Alessio Polvani: Writing – original draft, Visualization, Investigation, Formal analysis, Conceptualization. **Raffaello Nardin:** Writing – review & editing, Formal analysis. **Xinyu Liu:** Software, Formal analysis. **Francesco Di Grazia:** Writing – review & editing, Visualization. **Amedeo Boldrini:** Writing – review & editing. **Riccardo Gaetano Cirrone:** Writing – review & editing. **Luisa Galgani:** Writing – review & editing. **Gabriella Tamasi:** Writing – review & editing. **Steven A. Loiselle:** Writing – original draft, Supervision, Project administration, Investigation, Formal analysis.

Declaration of competing interest

The authors declare that they have no known competing financial interests or personal relationships that could have appeared to influence the work reported in this paper.

Acknowledgements

Our thanks go to the cooperation of Riccardo Mari, Francesco Vesprini, Vincenzo Fratello, Francesco Bonucci, Lorenzo Facci and Iacopo Moliterno for the contribution in the field work and laboratory analysis. We also thank the collaboration of CS4rivers. The researchers who contributed to this study received funding from the MoRe4Nature project (EU Horizon grant agreement No. 101133983).

Appendix A. Supplementary data

Supplementary data to this article can be found online at https://doi.org/10.1016/j.envpol.2026.127858.

Data availability

Data will be made available on request.

References

Ali, H., Khan, E., Ilahi, I., 2019. Environmental chemistry and ecotoxicology of hazardous heavy metals: Environmental persistence, toxicity, and bioaccumulation. J. Chem. 2019, 1–14. https://doi.org/10.1155/2019/6730305.

ARPAT, 2022. Monitoraggio ambientale dei corpi idrici superficiali (fiumi, laghi, acque di transizione) – triennio 2019–2021. Agenzia Regionale per la Protezione Ambientale Della Toscana (ARPAT).

ARPAT, 2023. Valori limite per le acque ad uso umano. Agenzia Regionale per la Protezione Ambientale Della Toscana (ARPAT). https://www.arpat.toscana.it/temi-ambientali/acqua/acque-ad-uso-umano/ac_usoumano_limiti.html.

Badeenezhad, A., Soleimani, H., Shahsavani, S., Parseh, I., Mohammadpour, A., Azadbakht, O., Javanmardi, P., Faraji, H., Babakrpur Nalosi, K., 2023. Comprehensive health risk analysis of heavy metal pollution using water quality indices and Monte Carlo simulation in R software. Sci. Rep. 13, 15817. https://doi.org/10.1038/s41598-023-43161-3.

Baken, S., Degryse, F., Verheyen, L., Merckx, R., Smolders, E., 2011. Metal complexation properties of freshwater dissolved organic matter are explained by its aromaticity and by anthropogenic ligands. Environ. Sci. Technol. 45, 2584–2590. https://doi.org/10.1021/es103532a.

Benito, G., Macklin, M.G., Zielhofer, C., Jones, A.F., Machado, M.J., 2015. Holocene flooding and climate change in the Mediterranean. Catena 130, 13–33. https://doi.org/10.1016/j.catena.2014.11.014.

Bhattacharya, R., Osburn, C.L., 2021. Chromophoric dissolved organic matter composition and load from a coastal river system under variable flow regimes. Sci. Total Environ. 760, 143414. https://doi.org/10.1016/j.scitotenv.2020.143414.

Bieroza, M.Z., Heathwaite, A.L., 2015. Seasonal variation in phosphorus concentration–discharge hysteresis inferred from high-frequency *in situ* monitoring. J. Hydrol. (Amst.) 524, 333–347. https://doi.org/10.1016/j.jhydrol.2015.02.036.

Chen, L., Zhuang, W.-E., Yang, L., 2022. Critical evaluation of the interaction between fluorescent dissolved organic matter and Pb(II) under variable environmental conditions. Chemosphere 307, 135875. https://doi.org/10.1016/j.chemosphere.2022.135875.

Bishop, I., Boldrini, A., Clymans, W., Hall, C., Moorhouse, H., Parkinson, S., Scott-Somme, K., Thornhill, I., Loiselle, S., 2025. FreshWater watch: Investigating the health of freshwater ecosystems, from the bottom up. Citiz. Sci. Theory Pr. 10, 2. https://doi.org/10.5334/cstp.754.

Briffa, J., Sinagra, E., Blundell, R., 2020. Heavy metal pollution in the environment and their toxicological effects on humans. Heliyon 6, e04691. https://doi.org/10.1016/j.heliyon.2020.e04691.

Chen, X., Du, J., Kanwal, S., Yang, Z.-J., Zheng, L.-L., Wang, J., Wen, J., Zhang, D.-W., 2023. A low-cost and portable fluorometer based on an optical pick-up unit for chlorophyll-a detection. Talanta 269, 125447. https://doi.org/10.1016/j.talanta.2023.125447.

Chiarantini, L., Benvenuti, M., Beutel, M., Costagliola, P., Covelli, S., Gabbani, G., Lattanzi, P., Pandeli, E., Paolieri, M., Petranich, E., Rimondi, V., 2016. Mercury and arsenic in stream sediments and surface waters of the orcia river basin, southern Tuscany, Italy. Water Air Soil Pollut. 227. https://doi.org/10.1007/s11270-016-3110-x.

Coble, P.G., 1996. Characterization of marine and terrestrial DOM in seawater using excitation-emission matrix spectroscopy. Mar. Chem. 51, 325–346. https://doi.org/10.1016/0304-4203(95)00062-3.

Cory, R.M., Kaplan, L.A., 2012. Biological lability of streamwater fluorescent dissolved organic matter. Limnol. Oceanogr. 57, 1347–1360. https://doi.org/10.4319/lo.2012.57.5.1347.

Derrien, M., Choi, H., Jardé, E., Shin, K.-H., Hur, J., 2020. Do early diagenetic processes affect the applicability of commonly-used organic matter source tracking tools? An assessment through controlled degradation end-member mixing experiments. Water Res. 173, 115588. https://doi.org/10.1016/j.watres.2020.115588.

Dini, A., Rielli, A., Di Giuseppe, P., Ruggieri, G., Boschi, C., 2024. The ophiolite-hosted Cu-Zn VMS deposits of Tuscany (Italy). Minerals 14, 273. https://doi.org/10.3390/min14030273.

Dong, L., Zhang, J., Guo, Z., Li, M., Wu, H., 2022. Distributions and interactions of dissolved organic matter and heavy metals in shallow groundwater in Guanzhong basin of China. Environ. Res. 207, 112099. https://doi.org/10.1016/j.envres.2021.112099.

European Commission, 2008. Directive 2008/105/EC on environmental quality standards in the field of water policy. Off. J. Eur. Union L 348, 84–97.

European Commission, 2023. EU Mission: Restore our Ocean and Waters. European Union. https://research-and-innovation.ec.europa.eu/funding/funding-opportunities/funding-programmes-and-open-calls/horizon-europe/eu-missions-horizon-europe/restore-our-ocean-and-waters_en.

Fornasaro, S., Morelli, G., Costagliola, P., Rimondi, V., Lattanzi, P., Fagotti, C., 2022. Total mercury mass load from the Paglia-Tiber River system: the contribution to Mediterranean Sea Hg budget. Toxics 10, 395. https://doi.org/10.3390/toxics10070395.

Frangipane, A., Paris, E., 1994. Long-term variability of sediment transport. In: Variability in Stream Erosion and Sediment Transport (Proceedings of the Canberra Symposium, December 1994), vol. 224. International Association of Hydrological Sciences, Wallingford, UK, pp. 317–324.

Gabor, R.S., Burns, M.A., Lee, R.H., Elg, J.B., Kemper, C.J., Barnard, H.R., McKnight, D. M., 2015. Influence of leaching solution and catchment location on the fluorescence of water-soluble organic matter. Environ. Sci. Technol. 49, 4425–4432. https://doi.org/10.1021/es504881t.

Guo, W., Xu, J., Wang, J., Wen, Y., Zhuo, J., Yan, Y., 2010. Characterization of dissolved organic matter in urban sewage using excitation emission matrix fluorescence spectroscopy and parallel factor analysis. J. Environ. Sci. (China) 22, 1728–1734. https://doi.org/10.1016/s1001-0742(09)60312-0.

Italian National Institute of Statistics (ISTAT), 2021. Risultati del Censimento permanente della popolazione. Available at: https://www.istat.it/statistiche-per-temi/censimenti/popolazione-e-abitazioni/risultati/.

Kannel, P.R., Lee, S., Kanel, S.R., Khan, S.P., 2007. Chemometric application in classification and assessment of monitoring locations of an urban river system. Anal. Chim. Acta 582, 390–399. https://doi.org/10.1016/j.aca.2006.09.006.

Kikuchi, T., Fujii, M., Terao, K., Jiwei, R., Lee, Y.P., Yoshimura, C., 2017. Correlations between aromaticity of dissolved organic matter and trace metal concentrations in natural and effluent waters: a case study in the Sagami River Basin. Japan. Sci. Total Environ. 576, 36–45. https://doi.org/10.1016/j.scitotenv.2016.10.068.

Li, D., Wang, Z., Yang, Y., Luo, M., Fang, S., Liu, H., Chai, J., Zhang, H., 2023. Characterization of copper binding to different molecular weight fractions of dissolved organic matter in surface water. J. Environ. Manag. 341, 118067. https://doi.org/10.1016/j.jenvman.2023.118067.

Li, W., Lu, L., Du, H., 2024. Deciphering DOM-metal binding using EEM-PARAFAC: mechanisms, challenges, and perspectives. Environ. Sci. Pollut. Res. Int. 31, 14388–14405. https://doi.org/10.1007/s11356-024-32072-z.

Liang, E., Li, J., Li, B., Liu, S., Ma, R., Yang, S., Cai, H., Xue, Z., Wang, T., 2023. Roles of dissolved organic matter (DOM) in shaping the distribution pattern of heavy metal in the Yangtze River. J. Hazard. Mater. 460, 132410. https://doi.org/10.1016/j.jhazmat.2023.132410.

Lin, H., Xu, H., Cai, Y., Belzile, C., Macdonald, R.W., Guo, L., 2021. Dynamic changes in size-fractionated dissolved organic matter composition in a seasonally ice-covered Arctic River. Limnol. Oceanogr. 66, 3085–3099. https://doi.org/10.1002/lno.11862.

Linlin, W., Xuan, Z., Meng, Z., 2011. Removal of dissolved organic matter in municipal effluent with ozonation, slow sand filtration and nanofiltration as high quality pre-treatment option for artificial groundwater recharge. Chemosphere 83, 693–699. https://doi.org/10.1016/j.chemosphere.2011.02.022.

Liu, M., Han, X., Guo, L., Ding, H., Lang, Y., 2024. Effects of Cu(II)-DOM complexation on DOM degradation: insights from spectroscopic evidence. Sci. Total Environ. 921, 170928. https://doi.org/10.1016/j.scitotenv.2024.170928.

Liu, X., Bannatyne, L., Boldrini, A., Polvani, A., Cirrone, R., Galgani, L., Woods, S., Warner, S., Loiselle, S., 2025. Realtime fluorescence organic matter indicators for early warning of river pollution sources. Ecol. Indic. 179, 114214. https://doi.org/10.1016/j.ecolind.2025.114214.

Ma, Y., Li, S., 2020. Spatial and temporal comparisons of dissolved organic matter in river systems of the Three Gorges Reservoir region using fluorescence and UV-Visible spectroscopy. Environ. Res. 189, 109925. https://doi.org/10.1016/j.envres.2020.109925.

Martin, Y.E., Johnson, E.A., 2012. Biogeosciences survey: studying interactions of the biosphere with the lithosphere, hydrosphere and atmosphere. Prog. Phys. Geogr. 36, 833–852. https://doi.org/10.1177/0309133312457107.

Mohinuzzaman, M., Mowa, J., Kabir, M.M., Chowdhury, M.A.Z., Nesha, M., Mostofa, K. M.G., Niloy, N.M., Shammi, M., Tareq, S.M., 2025. Water quality and fluorescent dissolved organic matter dynamics of Dhaleshwari River. Front. Water 7. https://doi.org/10.3389/frwa.2025.1507254.

Monaci, F., Ancora, S., Bianchi, N., Bonini, I., Paoli, L., Loppi, S., 2021. Combined use of native and transplanted moss for post-mining characterization of metal(loid) river contamination. Sci. Total Environ. 750, 141669. https://doi.org/10.1016/j.scitotenv.2020.141669.

Mostofa, K.M.G., Yoshioka, T., Konohira, E., Tanoue, E., 2007. Dynamics and characteristics of fluorescent dissolved organic matter in the groundwater, river and lake water. Water Air Soil Pollut. 184, 157–176. https://doi.org/10.1007/s11270-007-9405-1.

Murphy, K.R., Stedmon, C.A., Graeber, D., Bro, R., 2013. Fluorescence spectroscopy and multi-way techniques. PARAFAC. Anal. Methods 5, 6557. https://doi.org/10.1039/c3ay41160e.

Nannoni, A., Morelli, G., Lattanzi, P., Fagotti, C., Friani, R., Fornasaro, S., Ciani, F., Manca, R., Monnanni, A., Rimondi, V., Costagliola, P., 2025. Toxic trace elements transport in stream sediments from the world-class Monte Amiata Hg mining district: potential impact to the Mediterranean Sea. Environ. Pollut. 372, 126088. https://doi.org/10.1016/j.envpol.2025.126088.

Nguyen, T.N., Takaoka, M., Kusakabe, T., Shiota, K., 2024. Assessing the complexation of dissolved organic matter with heavy metals (Cu2+, Pb2+) in leachate from an old Japanese landfill site using fluorescence quenching. Environ. Sci. Pollut. Res. Int. 31, 52253–52266. https://doi.org/10.1007/s11356-024-34676-x.

Pagnanelli, F., Moscardini, E., Giuliano, V., Toro, L., 2004. Sequential extraction of heavy metals in river sediments of an abandoned pyrite mining area: pollution detection and affinity series. Environ. Pollut. 132, 189–201. https://doi.org/10.1016/j.envpol.2004.05.002.

Poulin, B.A., Ryan, J.N., Aiken, G.R., 2014. Effects of iron on optical properties of dissolved organic matter. Environ. Sci. Technol. 48, 10098–10106. https://doi.org/10.1021/es502670r.

Rinklebe, J., Shaheen, S.M., 2014. Assessing the mobilization of cadmium, lead, and nickel using a seven-step sequential extraction technique in contaminated floodplain soil profiles along the central Elbe river, Germany. Water Air Soil Pollut. 225. https://doi.org/10.1007/s11270-014-2039-1.

Saar, R.A., Weber, J.H., 1982. Fulvic acid: modifier of metal-ion chemistry. Environ. Sci. Technol. 16, 510A. https://doi.org/10.1021/es00103a723, 7A.

Sanna, V.S., Di Grazia, F., Capineri, C., Polvani, A., 2025. Citizen Science for transition to sustainability and SDG monitoring in an Italian river basin. Int. J. E-plan. Res. 13, 1–30. https://doi.org/10.4018/ijepr.366585.

Servizio Idrologico Regionale della Toscana, 2024. Archivio dati idrologici e pluviometrici. Regione Toscana. https://www.sir.toscana.it/archivio/scheda_dati.php.

Stedmon, C.A., Markager, S., 2005. Tracing the production and degradation of autochthonous fractions of dissolved organic matter by fluorescence analysis. Limnol. Oceanogr. 50, 1415–1426. https://doi.org/10.4319/lo.2005.50.5.1415.

Tchounwou, P.B., Yedjou, C.G., Patlolla, A.K., Sutton, D.J., 2012. Heavy metal toxicity and the environment. Exper. Suppl. (Basel) 101, 133–164. https://doi.org/10.1007/978-3-7643-8340-4_6.

Tedetti, M., Joffre, P., Goutx, M., 2013. Development of a field-portable fluorometer based on deep ultraviolet LEDs for the detection of phenanthrene- and tryptophan-like compounds in natural waters. Sens. Actuators B Chem. 182, 416–423. https://doi.org/10.1016/j.snb.2013.03.052.

Thornes, J.B., et al., 2009. Hydrology, river regimes, and sediment yield. In: The Physical Geography of the Mediterranean, first ed. Oxford University Press, Oxford, pp. 229–253.

Wang, Y., Zhang, D., Shen, Z.-Y., Feng, C.-H., Zhang, X., 2015. Investigation of the interaction between as and Sb species and dissolved organic matter in the Yangtze Estuary, China, using excitation-emission matrices with parallel factor analysis. Environ. Sci. Pollut. Res. Int. 22, 1819–1830. https://doi.org/10.1007/s11356-014-3380-z.

Wang, X., Tong, Y., Chang, Q., Lu, J., Ma, T., Zhou, F., Li, J., 2021. Source identification and characteristics of dissolved organic matter and disinfection by-product formation potential using EEM-PARAFAC in the Manas River, China. RSC Adv. 11, 28476–28487. https://doi.org/10.1039/d1ra03498g.

Wang, Z., Han, R., Muhammad, A., Guan, D.-X., Zama, E., Li, G., 2022. Correlative distribution of DOM and heavy metals in the soils of the Zhangxi watershed in Ningbo city, East of China. Environ. Pollut. 299, 118811. https://doi.org/10.1016/j.envpol.2022.118811.

World Health Organization, 2022. Guidelines for drinking-water Quality, Fourth Ed., Incorporating the 1st and 2nd Addenda. WHO Press, Geneva, Switzerland. https://www.who.int/publications/i/item/9789240045064.

Yamashita, Y., Jaffé, R., 2008. Characterizing the interactions between trace metals and dissolved organic matter using excitation-emission matrix and parallel factor analysis. Environ. Sci. Technol. 42, 7374–7379. https://doi.org/10.1021/es801357h.

Yan, X., Du, W., Ma, C., Cheng, S., Li, X., 2020. Humic acid adsorption behavior and mechanism comparison between biochars and activated carbon. Desalination Water Treat. 173, 213–222. https://doi.org/10.5004/dwt.2020.24825.

Yang, B., Cheng, X., Zhang, Y., Li, W., Wang, J., Tian, Z., Du, E., Guo, H., 2021. Staged assessment for the involving mechanism of humic acid on enhancing water decontamination using H2O2-Fe(III) process. J. Hazard. Mater. 407, 124853. https://doi.org/10.1016/j.jhazmat.2020.124853.

Yang, B., Xu, W., Zhao, W., 2026. Multi-scale mechanisms and environmental implications of dissolved organic matter-metal ions interactions in aquatic environments: a review. Water Res. 288, 124563. https://doi.org/10.1016/j.watres.2025.124563.

Zhang, X., Cai, X., Wang, Z., Yang, X., Li, S., Liang, G., Xie, X., 2021. Insight into metal binding properties of biochar-derived DOM using EEM-PARAFAC and differential absorption spectra combined with two-dimensional correlation spectroscopy. Environ. Sci. Pollut. Res. Int. 28, 13375–13393. https://doi.org/10.1007/s11356-020-11573-7.

Zhu, L., Zhao, Y., Bai, S., Zhou, H., Chen, X., Wei, Z., 2020. New insights into the variation of dissolved organic matter components in different latitudinal lakes of northeast China. Limnol. Oceanogr. 65, 471–481. https://doi.org/10.1002/lno.11316.

Zhu, C., Wu, K., Xu, D., Tang, X., Hu, Y., Zhang, M., Hassan, M.T., Chen, Y., 2024. Comprehensive insights into the occurrence characteristics of dissolved organic matter and its indication for heavy metals in drinking water sources. Environ. Pollut. Bioavailab. 36. https://doi.org/10.1080/26395940.2024.2367429.